

Propagation of weakly stretched premixed spherical spray flames in localized homogeneous and heterogeneous reactants ^{EP}

Cite as: Phys. Fluids **32**, 123302 (2020); <https://doi.org/10.1063/5.0031638>

Submitted: 02 October 2020 . Accepted: 03 November 2020 . Published Online: 01 December 2020

Qiang Li (李强),  Huangwei Zhang (张黄伟), and  Chang Shu (舒昌)

COLLECTIONS

 This paper was selected as an Editor's Pick



[View Online](#)



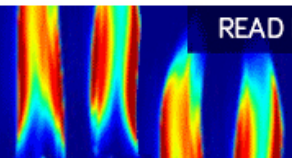
[Export Citation](#)



[CrossMark](#)

AIP Advances
Fluids and Plasmas Collection

READ NOW



Propagation of weakly stretched premixed spherical spray flames in localized homogeneous and heterogeneous reactants

Cite as: Phys. Fluids 32, 123302 (2020); doi: 10.1063/5.0031638

Submitted: 2 October 2020 • Accepted: 3 November 2020 •

Published Online: 1 December 2020



View Online



Export Citation



CrossMark

Qiang Li (李强), Huangwei Zhang (张黄伟),^{a)}  and Chang Shu (舒昌) 

AFFILIATIONS

Department of Mechanical Engineering, National University of Singapore, 9 Engineering Drive 1, Singapore 117576, Republic of Singapore

^{a)} Author to whom correspondence should be addressed: huangwei.zhang@nus.edu.sg. Tel.: +65 6516 2557

ABSTRACT

Propagation of weakly stretched spherical flames in partially pre-vaporized fuel sprays is theoretically investigated in this work. A general theory is developed to describe flame propagation speed, flame temperature, droplet evaporation onset, and completion locations. The influences of liquid fuel and gas mixture properties on spherical spray flame propagation are studied. The results indicate that the spray flame propagation speed is enhanced with increased droplet mass loading and/or evaporation heat exchange coefficient (or evaporation rate). Opposite trends are found when the latent heat is high due to strong evaporation heat absorption. Fuel vapor and temperature gradients are observed in the post-flame evaporation zone of heterogeneous flames. The evaporation completion front location considerably changes with flame radius. For larger droplet loading and a smaller evaporation rate, the fuel droplet tends to complete evaporation behind the flame front. Flame bifurcation occurs with high droplet mass loading under large latent heat, leading to multiplicity of flame propagation speed, droplet evaporation onset, and completion fronts. The flame enhancement or weakening effects by the fuel droplet sprays are revealed by the enhanced or suppressed heat and mass diffusion process in the pre-flame zone. Besides, for heterogeneous flames, heat and mass diffusion in the post-flame zone also exists. The mass diffusion for both homogeneous and heterogeneous flames is enhanced with a decreased Lewis number. The magnitude of the Markstein length is considerably reduced with increased droplet loading. Moreover, post-flame droplet burning behind the heterogeneous flame influences the flame propagation speed and Markstein length when the liquid fuel loading is relatively low.

Published under license by AIP Publishing. <https://doi.org/10.1063/5.0031638>

I. INTRODUCTION

Liquid fuel is predominantly used in many combustion applications, e.g., aero-engines and rocket engines. High-efficiency and low-emission spray combustion devices are in high demand nowadays. To achieve this, it is significant to first clarify the fundamental aspects of two-phase combustion, and one of them is flame initiation and propagation in sprayed fuel droplets.

The effects of fuel droplet properties on spray flame propagation have been extensively studied. For instance, Mizutani and Nakajima^{1,2} observed that adding kerosene droplets intensifies the propane/air combustion. However, it is also found that there exist appropriate droplet quantities for combustion enhancement.¹ Moreover, Myers and Lefebvre³ studied six liquid fuel sprays and

found that the flame speed is inversely proportional to the mean droplet diameter above some critical value and increases with the overall equivalence ratio. Hayashi and Kumagai⁴ observed that the flame speed decreases with liquid fuel loading in overall fuel-lean mixtures. Nomura *et al.*⁵⁻⁷ found that the flame speed of fuel (methanol and ethanol) droplet-vapor-air mixtures exceeds that of premixed gaseous of the same total equivalence ratio in the fuel-lean and fuel-rich regions of the total equivalence ratio. Moreover, Atzler *et al.*⁸ observed that the burning rates of *iso*-octane/air aerosols are strongly affected by the droplet diameter when the equivalence ratio is high. Similar results are also achieved by Bradley *et al.*,⁹ through analyzing the equivalence ratio and droplet size effects on flame propagation speeds of *iso*-octane and ethanol aerosols. It is also seen by Neophytou and Mastorakos¹⁰ that the high flame speed

of *n*-heptane and *n*-decane is achieved with small droplet diameters and long residence time under fuel-lean condition. Ren *et al.* numerically studied spray flame propagation behaviors involved in vortices of supersonic mixing layers,^{11,12} and they found that the vortex dynamics and elevated pressure considerably affect spray combustion.

The foregoing influences of the liquid fuel sprays on flame propagation are related to the droplet behaviors, e.g., movement, heating, and evaporation.^{13,14} It is observed through spray combustion experiments^{4,8,15–19} that small-sized droplets can complete evaporation in the preheating zone or immediately around the flame front, but relatively large droplets penetrate through the flame front and continue vaporizing in the post-flame zone. Three spray flame propagation modes are identified from the droplet-level OH* chemiluminescence and OH-PLIF images by de Oliveira and Mastorakos,¹⁵ including droplet propagation, inter-droplet propagation, and gaseous-like propagation modes. Furthermore, Thimothée *et al.*¹⁹ studied the passage of liquid droplets through a spherical flame and found that the droplet size and inter-droplet distance are the most important controlling factors. These peculiar phenomena have also been observed in Direct Numerical Simulation (DNS) of spray combustion.^{20–22}

However, how the droplet distribution and flame propagation intrinsically interact with each other is still not well understood. This is partly caused by the comprehensive (hence complicated) interphase coupling in spray flames, and therefore, it is challenging to underpin the mechanism behind the observed flame/droplet behaviors. Theoretical analysis is deemed a powerful tool for two-phase combustion studies since it can retain or isolate the most relevant factors in the studied problem, thereby highlighting physical relevance and ensuring conclusion generality. For instance, Lin *et al.*^{23,24} developed a theoretical model for fully and partially pre-vaporized burning sprays. Greenberg^{25,26} derived an evolution equation for a laminar flame propagation into fuel spray cloud, considering finite-rate evaporation and droplet drag effects. However, in the above studies,^{23–26} the flame–droplet interactions are not studied. Recently, Han and Chen²⁷ further examined the influences of finite-rate evaporation on spray flame propagation and ignition and found that the flame propagation speed, Markstein length, and minimum ignition energy are strongly affected by droplet loading and the evaporation rate. Nonetheless, in their work,

the droplets are assumed to be distributed in the full burned and unburned areas. With a more general theory, Li *et al.*²⁸ considered the droplet evaporation completion before or after a steadily propagating planar spray flame front and found that differentiated droplet distributions have significant importance on flame propagation. Zhuang and Zhang²⁹ theoretically analyzed the consistently varying droplet distributions in a propagating spherical flame, but only fine water sprays are studied. Therefore, the interactions between liquid fuel sprays and propagating spherical flames merit further investigation.

In this work, we aim to conduct theoretical analysis on propagation of a spherical spray flame in partially pre-vaporized fuel sprays. Dynamic droplet distributions with a propagating flame front will be described in our model, characterized by evolving droplet evaporation onset and completion locations. This leads to localized homogeneous and heterogeneous reactants at the flame front. The influences of liquid fuel and gas mixture properties will be examined, including evaporation heat transfer coefficient (or evaporation rate), droplet mass loading, latent heat of vaporization, and Lewis number. The rest of this paper is structured as below. The physical and mathematical models are presented in Sec. II. The analytical solutions are listed in Sec. III. The results will be discussed in Sec. IV. Section V closes the paper with main conclusions.

II. PHYSICAL AND MATHEMATICAL MODEL

A. Physical model

In this work, one-dimensional spherical flames in partially pre-vaporized fuel sprays will be studied. Two general scenarios are considered, with evaporating droplets: (1) in both pre- and post-flame zones and (2) in the pre-flame zone only. The sketches of their physical models are shown in Figs. 1(a) and 1(b), respectively. There are three different characteristic locations for liquid and gas phases in our model, including the gaseous flame front (R_f), droplet evaporation onset (R_v), and completion (R_c) fronts. Specifically, R_v corresponds to the location where the droplet starts to evaporate. The droplets are just heated up to boiling temperature, and behind this front (i.e., $R < R_v$), the droplet temperature maintains the boiling temperature and evaporation continues.^{27,29–32} The evaporation

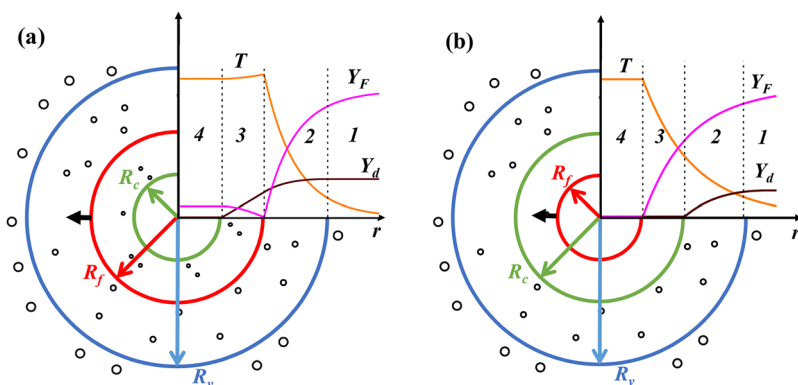


FIG. 1. Schematic of the outwardly propagating spherical flame in liquid fuel mists: (a) heterogeneous flame and (b) homogeneous flame. Circle: fuel droplet. Red line: flame front (R_f); green line: evaporation completion front (R_c); blue line: evaporation onset front (R_v). Black arrow: flame propagation direction.

onset front R_v is always before the flame front R_f , indicating that onset of droplet vaporization spatially precedes the gaseous combustion. Moreover, R_c denotes the location at which all the droplets are critically vaporized. When $R < R_c$, no droplets are left, and hence, their effects on the gaseous flame diminish.

In Fig. 1(a), the evaporation completion front lies after the flame front (i.e., $R_c < R_f < R_v$). The local mixture around the flame front R_f is composed of gaseous vapor and evaporating fuel droplets. In Fig. 1(b), the evaporation completion front is located before the flame front (i.e., $R_f < R_c < R_v$), and the mixture around the flame front is purely gaseous since all the droplets have been gasified into vapor there. For brevity, hereafter, we term the first and second cases as heterogeneous (abbreviated as “HT”) and homogeneous (“HM”) flames, respectively. As shown in Fig. 1, for both flames, zone 1 represents the pre-vaporization zone before R_v . Zone 2 indicates the pre-flame evaporation zone before R_f for the heterogeneous flame and before R_c for the homogeneous flame. As for zone 3, it represents the post-flame evaporation zone before R_c for the heterogeneous flame and pre-flame zone without evaporation for the homogeneous flame. Meanwhile, zone 4 is the post-flame zone without evaporation for both flames. In the following, we will develop a general theory to describe propagation and transition of homogeneous and heterogeneous spherical spray flames, considering consistently evolving fuel droplets with the moving reaction front. In this model, introduction of multiple liquid droplet zones renders it more general, thereby better mimicking practical spray flame problems compared with previous studies.^{25,27,31}

B. Governing equation

For gaseous flames, the well-known diffusive-thermal model^{33,34} is adopted, with which the thermal and transport properties (e.g., density, thermal conductivity, and heat capacity) are assumed to be constant and the convection flux is absent. This model has been used in numerous studies on gaseous and two-phase flames.^{27,29,31,32,35,36} One-step chemistry is considered, i.e., $F + O \rightarrow P$, with F , O , and P being the fuel vapor, oxidizer, and product, respectively. Globally fuel-lean mixture (i.e., total equivalence ratios of fuel vapor and droplets are below unity) is studied in this work. Therefore, the equations for the gas temperature and fuel mass fraction are

$$\tilde{\rho}_g \tilde{C}_{p,g} \frac{\partial \tilde{T}}{\partial \tilde{t}} = \frac{1}{\tilde{r}^2} \frac{\partial}{\partial \tilde{r}} \left(\tilde{r}^2 \tilde{\lambda}_g \frac{\partial \tilde{T}}{\partial \tilde{r}} \right) + \tilde{q}_c \tilde{\omega}_c - \tilde{q}_v \tilde{\omega}_v + \alpha \tilde{q}_c \tilde{\omega}, \quad (1)$$

$$\tilde{\rho}_g \frac{\partial \tilde{Y}_F}{\partial \tilde{t}} = \frac{1}{\tilde{r}^2} \frac{\partial}{\partial \tilde{r}} \left(\tilde{r}^2 \tilde{\rho}_g \tilde{D}_F \frac{\partial \tilde{Y}_F}{\partial \tilde{r}} \right) - \tilde{\omega}_c + \tilde{\omega}_v - \alpha \tilde{\omega}, \quad (2)$$

where the tilde symbol \sim is used to indicate that the variables are dimensional. \tilde{t} and \tilde{r} are, respectively, the temporal and spatial coordinates. \tilde{T} , $\tilde{\rho}_g$, $\tilde{C}_{p,g}$, and $\tilde{\lambda}_g$ are the gas temperature, density, heat capacity, and thermal conductivity, respectively. \tilde{Y}_F and \tilde{D}_F are the mass fraction and molecular diffusivity of the fuel. \tilde{q}_c is the reaction heat release per unit mass of the fuel. \tilde{q}_v is the latent heat of vaporization of liquid fuel, while $\tilde{\omega}_v$ is the evaporation rate of the fuel droplet. The chemical reaction rate $\tilde{\omega}_c$ in Eq. (1) takes the Arrhenius form

$$\tilde{\omega}_c = \tilde{\rho}_g \tilde{A} \tilde{Y}_F \exp(-\tilde{E}/\tilde{R}^0 \tilde{T}). \quad (3)$$

Here, \tilde{A} is the pre-exponential factor, \tilde{E} is the activation energy for the reaction, and \tilde{R}^0 is the universal gas constant.

The governing equations for the gas phase are similar to those in our previous work,²⁸ but droplet burning behind the flame front is considered in this work. Specifically, in Eqs. (1) and (2), α is an indicator for post-flame droplet burning in heterogeneous flames.²⁷ Specifically, $\alpha = 0$ indicates that droplet burning in the post-flame zone is neglected, practically corresponding to the situations, e.g., when the local equivalence ratio is beyond the flammability limit and/or the vapor/oxidizer is not well mixed.¹⁵ On the contrary, when $\alpha = 1$, we assume that the fuel vapor is totally consumed by the local diffusion combustion surrounding individual droplets in the post-flame zone.¹⁵ In this case, the last terms in Eqs. (1) and (2) are sink terms, only applicable for the post-flame evaporation zone [zone 3 in Fig. 1(a)] of the heterogeneous flame. The droplet burning term $\tilde{\omega}$ reads

$$\tilde{\omega} = \tilde{\omega}_v H(\tilde{R}_f - \tilde{r}). \quad (4)$$

$H(\cdot)$ is the Heaviside function. Note that when $\alpha = 1$, $\tilde{\omega} = \alpha \tilde{\omega}_v$ is valid at the right side of Eq. (2), which implies that all the vaporized fuel behind the flame front \tilde{R}_f is reacted with the heat release of $\tilde{q}_c \tilde{\omega}$ in Eq. (1).

For liquid fuel droplets, we assume that they are uniformly monodispersed dilute spray in the initial pre-vaporized fuel/air mixture. The droplets are spherical, and their properties (e.g., density and heat capacity) are assumed to be constant. Due to the dilute droplet concentration, the inter-droplet collisions are not considered, and therefore, the diffusion of liquid droplets can be neglected. The above assumptions are also used in previous theoretical work on two-phase flames.^{23,37–39} Furthermore, in zone 1 (pre-vaporization, see Fig. 1), interphase thermal equilibrium is assumed, and hence, they have the same temperature.^{27,29–32} The Eulerian description is adopted for the liquid phase, and hence, the equation for droplet mass loading Y_d ($\equiv \tilde{N}_d \tilde{m}_d / \tilde{\rho}_g$) reads

$$\frac{\partial}{\partial \tilde{t}} \left(\frac{\tilde{N}_d \tilde{m}_d}{\tilde{\rho}_g} \right) = \frac{\partial Y_d}{\partial \tilde{t}} = -\frac{\tilde{\omega}_v}{\tilde{\rho}_g}, \quad (5)$$

where \tilde{N}_d is the droplet number density.

We assume that the heat transferred from the surrounding gas to the droplets is completely used for phase change, which is related to the latent heat of evaporation \tilde{q}_v .^{4,29,30,32} Therefore, $\tilde{\omega}_v$ in Eqs. (1), (2), (4), and (5) can be modeled as

$$\tilde{\omega}_v = \frac{\tilde{N}_d \tilde{s}_d \tilde{h} (\tilde{T} - \tilde{T}_v) H(\tilde{T} - \tilde{T}_v)}{\tilde{q}_v}, \quad (6)$$

where $\tilde{s}_d = \pi \tilde{d}^2$ is the surface area of a single droplet, \tilde{d} is the droplet diameter, Nu is the Nusselt number, and \tilde{T}_v is the boiling temperature of the liquid fuel. \tilde{h} is the heat transfer coefficient, estimated using the Ranz and Marshall correlation,⁴⁰

$$Nu = \frac{\tilde{h} \tilde{d}_p}{\tilde{\lambda}_g} = 2.0 + 0.6 Re^{1/2} Pr^{1/3}, \quad (7)$$

where Nu , Pr , and Re are the Nusselt number, Prandtl number, and particle Reynolds number, respectively. We can neglect the effect of particle Reynolds number due to the assumption of kinematic equilibrium, and therefore, $Nu \approx 2$. Accordingly, the evaporation rate $\tilde{\omega}_v$ can be re-written as

$$\tilde{\omega}_v = \tilde{N}_d \tilde{s}_d \tilde{\lambda}_g Nu (\tilde{T} - \tilde{T}_v) H(\tilde{T} - \tilde{T}_v) / (\tilde{d} \tilde{q}_v). \quad (8)$$

To render the analytical analysis more general, normalization of Eqs. (1), (2), and (5) can be performed, with the following non-dimensional parameters:

$$U = \frac{\tilde{u}}{\tilde{u}_b}, r = \frac{\tilde{r}}{\tilde{l}_{th}}, t = \frac{\tilde{t}}{\frac{\tilde{l}_{th}}{\tilde{u}_b}}, Y = \frac{\tilde{Y}}{\tilde{Y}_0}, T = \frac{\tilde{T} - \tilde{T}_0}{\tilde{T}_b - \tilde{T}_0}. \quad (9)$$

Here, \tilde{T}_0 and \tilde{Y}_0 denote the temperature and fuel mass fraction of the pre-vaporized pre-mixture, respectively. \tilde{u}_b , $\tilde{T}_b = \tilde{T}_0 + \tilde{q}_c \tilde{Y}_0 / \tilde{C}_{p,g}$, and $\tilde{l}_{th} = \tilde{D}_{th} / \tilde{u}_b$ are, respectively, the laminar flame speed, adiabatic flame temperature, and flame thickness based on the pre-vaporized pre-mixture. $\tilde{D}_{th} = \tilde{\lambda}_g / \tilde{\rho}_g \tilde{C}_{p,g}$ is the thermal diffusivity.

Following previous theoretical analysis for both gaseous flames and two-phase flames with dispersed liquid droplets,^{27,31,35,41–46} we adopt the quasi-steady state assumption in the moving coordinate system attached to the stably propagating flame front $R_f(t)$, i.e., $\eta = r - R_f(t)$. This assumption has been extensively validated by transient numerical simulations for gaseous spherical flames,^{35,41–43,47} in which the unsteady effects are found to have a negligible influence based on the budget analysis of diffusion, reaction, and convection terms in stably propagating spherical flames. Moreover, due to relatively dilute fuel droplet concentration, their influences on the reaction zone thickness are small, and therefore, gaseous combustion still dominates.^{27,30} In addition, due to the kinematic equilibrium between the two phases, the droplets approximately follow the carrier gas. Therefore, the non-dimensional equations (1), (2), and (5) can be written as

$$-U \frac{dT}{d\eta} = \frac{1}{(\eta + R_f)^2} \frac{d}{d\eta} \left[(\eta + R_f)^2 \frac{dT}{d\eta} \right] + \omega_c - q_v \omega_v + \alpha \bar{\omega}, \quad (10)$$

$$-U \frac{dY_F}{d\eta} = \frac{Le^{-1}}{(\eta + R_f)^2} \frac{d}{d\eta} \left[(\eta + R_f)^2 \frac{dY_F}{d\eta} \right] - \omega_c + \omega_v - \alpha \bar{\omega}, \quad (11)$$

$$-U \frac{dY_d}{d\eta} = -\omega_v, \quad (12)$$

where $U = dR_f/dt$ is the non-dimensional flame propagating speed. $q_v = \tilde{q}_v / [\tilde{C}_{p,g}(\tilde{T}_b - \tilde{T}_0)]$ is the normalized latent heat of vaporization. $Le = \tilde{D}_{th} / \tilde{D}_F$ is the Lewis number. The normalized chemical reaction rate ω_c reads

$$\omega_c = \frac{1}{2Le} Y_F Z^2 \exp \left[\frac{Z(T-1)}{\sigma + (1-\sigma)T} \right], \quad (13)$$

where Z is the Zel'dovich number and σ is the thermal expansion ratio. They are assumed to be $Z = 10$ and $\sigma = 0.15$, respectively, following Refs. 27, 29, 31, 32, 35, and 36.

The term ω_v in Eqs. (10)–(12) is the non-dimensional droplet evaporation rate, i.e.,

$$\omega_v = \frac{\Omega(T - T_v)}{q_v} H(T - T_v), \quad (14)$$

where T_v is the non-dimensional boiling temperature and assumed to be $T_v = 0.15$.^{27,48} The heat exchange coefficient Ω is

$$\Omega = \pi \tilde{N}_d \tilde{Nud} \tilde{D}_{th}^2 \tilde{u}_b^{-2}. \quad (15)$$

As shown in Eq. (15), Ω is a gross parameter associated with both gas and droplet properties.^{29,30} To avoid the nonlinearity in Eq. (12), the weak dependence of Ω on Y_d ($\Omega \sim Y_d^{1/3}$) is not considered, following Belyakov *et al.*³⁰

Typically, the droplet evaporation rate is a function of Sherwood number, Spalding mass transfer number, as well as gas and droplet properties (e.g., density and diameter). In the current study, since we assume that the kinematic equilibrium has been reached between the gaseous and droplet, the effect of the Sherwood number is small. Furthermore, since it is assumed that evaporation proceeds at the boiling temperature and constant atmospheric pressure, the fuel vapor at the droplet surface is relatively constant, and hence, the Spalding number would change slightly. The current model assumes energy balance between phase change and heat transfer from the gaseous mixture. Despite these, it is still physically comprehensive since it considers various effects of the gas and liquid phase properties as mentioned above. Therefore, the current evaporation model is expected to be sufficient. It should be noted that this model is different from the evaporation model used by Han and Chen.²⁷ For the latter, it takes the droplet mass loading into consideration, and hence, the exponential distributions of droplet loading distribution in both pre- and post-flame zones can be analytically derived. Therefore, strictly speaking, with that model, it is not possible to include the evaporation completion front where $Y_d = 0$ should be exactly satisfied.

For a fixed latent heat q_v , higher Ω indicates the faster droplet evaporation rate. Moreover, the normalized droplet burning term $\bar{\omega}$ in Eqs. (10) and (11) is

$$\bar{\omega} = \omega_v H(-\eta). \quad (16)$$

In the current work, propagation of spherical spray flames under the moderate or weak stretch rate will be investigated. Therefore, we assume that the reactive-diffusive structure of the spherical flame is quasi-planar [$R_f \gg 1$, $\eta \sim O(1)$]^{29,43,45,46,49} in this study. Its validity has been confirmed in Refs. 43 and 49. Therefore, the governing equations of gas and liquid phases are reduced to

$$\frac{d^2 T}{d\eta^2} + \left(\frac{2}{R_f} + U \right) \frac{dT}{d\eta} + \omega_c - q_v \omega_v + \alpha \bar{\omega} = 0, \quad (17)$$

$$\frac{d^2 Y_F}{d\eta^2} + \left(\frac{2}{R_f} + LeU \right) \frac{dY_F}{d\eta} - Le\omega_c + Le\omega_v - \alpha Le \bar{\omega} = 0, \quad (18)$$

$$-U \frac{dY_d}{d\eta} = -\omega_v. \quad (19)$$

C. Jump and boundary conditions

The non-dimensional boundary conditions for both gas phase (T and Y_F) and liquid phase (Y_d) at the left boundary (spherical center, $\eta = -R_f$) and the right boundary ($\eta \rightarrow +\infty$) are^{27,29–32}

$$\eta = -R_f: \quad \frac{dT}{d\eta} = 0, \quad \frac{dY_F}{d\eta} = 0, \quad Y_d = \begin{cases} 0, & \text{if } \eta_c \neq -R_f, \\ \delta_r, & \text{if } \eta_c = -R_f, \end{cases} \quad (20)$$

$$\eta \rightarrow +\infty: \quad T = 0, \quad Y_F = 1, \quad Y_d = \delta. \quad (21)$$

Here, δ is the initial mass loading of the fuel droplet in the fresh mixture. In Eq. (20), for Y_d , if $\eta_c \neq -R_f$, the droplets at the spherical center are fully vaporized and hence partially distributed behind the flame. Otherwise, they exist in the entire burned area corresponding to $\eta_c = -R_f$, and δ_r is the mass loading at the spherical center to be determined (will be discussed later). It can be seen from Eq. (21) that the normalized total mass fraction of fuel in the fresh mixture at $\eta \rightarrow +\infty$ is $1 + \delta$, which is assumed to correspond to the fuel-lean condition.

At the evaporation onset front, $\eta = \eta_v$, the gas temperature (T), fuel mass fraction (Y_F), and fuel droplet mass loading (Y_d) satisfy the following jump conditions:^{27,29–32}

$$T = T_v, \quad [T] = [Y_F] = \left[\frac{dY_F}{d\eta} \right] = 0, \quad Y_d = \delta, \quad (22)$$

where the square brackets, i.e., $[T] = T(\eta^+) - T(\eta^-)$, denote the difference between the variables at two sides of a location.

At the evaporation completion front, $\eta = \eta_c$, the jump conditions for the gas temperature (T), fuel mass fraction (Y_F), and droplet mass loading (Y_d) take the following form:³⁰

$$\begin{cases} [T] = [Y_F] = \left[\frac{dY_F}{d\eta} \right] = 0, & Y_d = 0, & \eta_c > 0, \\ [T] = 0, \quad \left. \frac{dT}{d\eta} \right|_+ = 0, & [Y_d] = 0, & -R_f < \eta_c < 0. \end{cases} \quad (23)$$

Here, the + symbol indicate the value is on the positive side of η_c , i.e., the left boundary of zone 3 in Fig. 1(a).

Large activation energy of the gas phase reaction is assumed in this study. This assumption has been successfully used for theoretical analysis of both gaseous^{35,41,42,47,50,51} and particle- or droplet-laden^{26,27,32,36–39} flames. It has been shown to be adequate to predict the main flame dynamics, such as ignition and propagation. In the limit of large activation energy, chemical reaction is confined at an infinitesimally thin sheet (i.e., $\eta = 0$). The corresponding jump conditions are

$$T = T_f, \quad Y_F = [Y_d] = 0, \quad (24)$$

$$-\left[\frac{dT}{d\eta} \right] = \frac{1}{Le} \left[\frac{dY_F}{d\eta} \right] = \left[\sigma + (1 - \sigma)T_f \right]^2 \exp \left[\frac{Z}{2} \left(\frac{T_f - 1}{\sigma + (1 - \sigma)T_f} \right) \right], \quad (25)$$

where T_f is the flame temperature.

It should be highlighted that there exist two critical cases that only involves three zones. They, respectively, correspond to the coincidence of the evaporation completion front with the spherical center ($\eta_c = -R_f$) and flame front ($\eta_c = 0$). The first is possible with the large droplet diameter, high initial liquid loading, or low evaporation rate, leading to droplet dispersion in the full post-flame zone.^{15,16} Accordingly, zone 4 [gaseous post-flame zone in Fig. 1(a)] is degenerated. The condition of $Y_d = \delta_r$ [see Eq. (20)] is enforced at the spherical center, and δ_r is solved as an eigenvalue of the problem, instead of η_c . Moreover, the second case, i.e., $\eta_c = 0$, corresponds to a critical condition between heterogeneous and homogeneous flames. Zone 3 is degenerated, which is the pre-flame (post-flame) evaporation zone in homogeneous (heterogeneous) flames. This is experimentally observed by Sulaiman *et al.*¹⁷ and de Oliveira and Mastorakos,¹⁵ in which well-sprayed fuel droplets are fully vaporized around the flame. For this case, the jump conditions at the flame

front [Eqs. (24) and (25)] are used, instead of those at $\eta = \eta_c$ given in Eq. (23). This limiting situation is also studied by Zhuang and Zhang³² for spherical flame propagation in fine water mists.

III. ANALYTICAL SOLUTION

Equations (17)–(19) with boundary and jump conditions [i.e., Eqs. (20)–(25)] can be solved analytically. The solutions for gas temperature T , fuel mass fraction Y_F , and droplet mass loading Y_d in four zones are presented in Sec. III A for general heterogeneous and homogeneous flames, i.e., $\eta_c \neq -R_f$ or 0. Moreover, the correlations for flame speed U , flame temperature T_f , evaporation onset location η_v , and completion location η_c under different flame radii R_f are derived in Sec. III B.

A. Distributions of T , Y_F , and Y_d

If the reactants around the flame front R_f are heterogeneous (including fuel vapors and droplets), the distributions of temperature T , fuel mass fraction Y_F , and droplet loading Y_d from zones 1 to 4 are (the number subscripts indicate different zones)

$$\begin{cases} T_1(\eta) = T_v e^{-\xi(\eta - \eta_v)}, \\ T_2(\eta) = T_v - \frac{T_v \xi \left[e^{\gamma_a(\eta - \eta_v)} - e^{\gamma_b(\eta - \eta_v)} \right]}{\gamma_a - \gamma_b}, \\ T_3(\eta) = T_v + \frac{T_f - T_v \left[\frac{e^{\chi_a(\eta - \eta_c)}}{\chi_a} - \frac{e^{\chi_b(\eta - \eta_c)}}{\chi_b} \right]}{\mu_a - \mu_b}, \\ T_4(\eta) = T_v + \frac{T_f - T_v \left(\frac{1}{\chi_a} - \frac{1}{\chi_b} \right)}{\mu_a - \mu_b}, \end{cases} \quad (26)$$

$$\begin{cases} Y_{F,1}(\eta) = 1 + \frac{I'_2(\eta_v)}{I'_1(\eta_v)} I_1(\eta) + G(\eta_v) I_1(\eta), \\ Y_{F,2}(\eta) = 1 + \frac{I'_2(\eta_v)}{I'_1(\eta_v)} I_1(\eta_v) + G(\eta_v) I_1(\eta) + I_2(\eta) - I_2(\eta_v), \\ Y_{F,3}(\eta) = -\frac{I'_3(\eta_c)}{I'_1(\eta_c)} I_1(\eta) + \frac{I'_3(\eta_c)}{I'_1(\eta_c)} I_1(0) + I_3(\eta) - I_3(0), \\ Y_{F,4}(\eta) = -\frac{I'_3(\eta_c)}{I'_1(\eta_c)} I_1(\eta_c) + \frac{I'_3(\eta_c)}{I'_1(\eta_c)} I_1(0) + I_3(\eta_c) - I_3(0), \end{cases} \quad (27)$$

$$\begin{cases} Y_{d,1}(\eta) = \delta, \\ Y_{d,2}(\eta) = \delta - \frac{\Omega T_v \xi R_f}{U q_v (\gamma_a - \gamma_b)} \left[\frac{e^{\gamma_a(\eta - \eta_v)} - 1}{\gamma_a} - \frac{e^{\gamma_b(\eta - \eta_v)} - 1}{\gamma_b} \right], \\ Y_{d,3}(\eta) = \frac{\Omega (T_f - T_v)}{U q_v (\mu_a - \mu_b)} \left[\frac{e^{\chi_a(\eta - \eta_c)} - 1}{\chi_a^2} - \frac{e^{\chi_b(\eta - \eta_c)} - 1}{\chi_b^2} \right], \\ Y_{d,4}(\eta) = 0, \end{cases} \quad (28)$$

where $\xi = (2 + R_f U)/R_f$, $\gamma_{a,b} = (-\xi \pm \sqrt{4\Omega + \xi^2})/2$, $\chi_{a,b} = (-\xi \pm \sqrt{4\Omega(1 - \alpha/q_v) + \xi^2})/2$, and $\mu_{a,b} = e^{-\chi_{a,b}\eta_c}/\gamma_{a,b}$. $I_1(\eta)$, $I_2(\eta)$, and $I_3(\eta)$ are

$$I_1(\eta) = -\frac{Re^{-\frac{2+LeR_f U}{R}\eta}}{2 + LeR_f U}, \quad (29)$$

$$I_2(\eta) = \frac{LeT_v(2 + R_f U)}{q_v(\gamma_a - \gamma_b)} \times \left[\frac{e^{\gamma_a(\eta - \eta_v)}}{\gamma_a(2 + \gamma_a R_f + LeR_f U)} - \frac{e^{\gamma_b(\eta - \eta_v)}}{\gamma_b(2 + \gamma_b R_f + LeR_f U)} \right], \quad (30)$$

$$I_3(\eta) = \frac{LeR_f \Omega (T_f - T_v)(\alpha - 1)}{q_v(\mu_a - \mu_b)} \times \left[\frac{e^{\chi_a(\eta - \eta_c)}}{\chi_a^2(2 + \chi_a R_f + LeR_f U)} - \frac{e^{\chi_b(\eta - \eta_c)}}{\chi_b^2(2 + \chi_b R_f + LeR_f U)} \right]. \quad (31)$$

$I'_1(\eta)$, $I'_2(\eta)$, and $I'_3(\eta)$ are, respectively, their first derivatives. In Eq. (27), $G(\eta_v)$ takes the following form:

$$G(\eta_v) = \frac{-1 - \frac{I'_2(\eta_v)}{I'_1(\eta_v)} I_1(\eta_v) + I_2(\eta_v) - I_2(0)}{I_1(0)}. \quad (32)$$

If the reactants around the flame front R_f are homogeneous (i.e., fuel vapors only), the distributions of T , Y_F , and Y_d from zones 1 to 4 are

$$\begin{cases} T_1(\eta) = T_v e^{-\xi(\eta - \eta_v)}, \\ T_2(\eta) = T_v - \frac{T_v \xi [e^{\gamma_a(\eta - \eta_v)} - e^{\gamma_b(\eta - \eta_v)}]}{\gamma_a - \gamma_b}, \\ T_3(\eta) = T_v - \frac{T_v \xi (\theta_a - \theta_b)}{\gamma_a - \gamma_b} - \frac{T_v (\gamma_a \theta_a - \gamma_b \theta_b)}{\gamma_a - \gamma_b} [1 - e^{-\xi(\eta - \eta_c)}], \\ T_4(\eta) = T_f, \end{cases} \quad (33)$$

$$\begin{cases} Y_{F,1}(\eta) = 1 + \frac{I'_2(\eta_v)}{I'_1(\eta_v)} I_1(\eta) - \mathcal{H}(\eta_v, \eta_c) I_1(\eta), \\ Y_{F,2}(\eta) = 1 + \frac{I'_2(\eta_v)}{I'_1(\eta_v)} I_1(\eta_v) - \mathcal{H}(\eta_v, \eta_c) I_1(\eta) + I_2(\eta) - I_2(\eta_v), \\ Y_{F,3}(\eta) = \left[\mathcal{H}(\eta_v, \eta_c) - \frac{I'_2(\eta_c)}{I'_1(\eta_c)} \right] [I_1(0) - I_1(\eta)], \\ Y_{F,4}(\eta) = 0, \end{cases} \quad (34)$$

$$\begin{cases} Y_{d,1}(\eta) = \delta, \\ Y_{d,2}(\eta) = \delta - \frac{\Omega T_v \xi R_f}{U q_v (\gamma_a - \gamma_b)} \left[\frac{e^{\gamma_a(\eta - \eta_v)} - 1}{\gamma_a} - \frac{e^{\gamma_b(\eta - \eta_v)} - 1}{\gamma_b} \right], \\ Y_{d,3}(\eta) = 0, \\ Y_{d,4}(\eta) = 0, \end{cases} \quad (35)$$

where $\theta_{a,b} = e^{\gamma_{a,b}(\eta_c - \eta_v)}$. In Eq. (34), $\mathcal{H}(\eta_v, \eta_c)$ has the following form:

$$\mathcal{H}(\eta_v, \eta_c) = \frac{1 + \frac{I'_2(\eta_v)}{I'_1(\eta_v)} I_1(\eta_v) + \frac{I'_2(\eta_c)}{I'_1(\eta_c)} [I_1(0) - I_1(\eta_c)] - I_2(\eta_v) + I_2(\eta_c)}{I_1(0)}. \quad (36)$$

B. Correlations for spherical flame and fuel sprays

The correlations between flame radius R_f , flame propagation speed, U and droplet characteristic locations, η_v and η_c , can be derived through the proper jump conditions in Sec. II C. If the reactants around the flame front R_f are heterogeneous, then the following correlation holds:

$$\frac{T_f - T_v}{\mu_a - \mu_b} (e^{-\chi_a \eta_c} - e^{-\chi_b \eta_c}) + \frac{\xi T_v}{\gamma_a - \gamma_b} (\gamma_a e^{-\gamma_a \eta_v} - \gamma_b e^{-\gamma_b \eta_v}) = Q(T_f), \quad (37)$$

$$\frac{G(\eta_v) I'_1(0) + I'_2(0) + \frac{I'_3(\eta_c)}{I'_1(\eta_c)} I'_1(0) - I'_3(0)}{Le} = Q(T_f), \quad (38)$$

$$T_v + \frac{\xi T_v}{\gamma_b - \gamma_a} (e^{-\gamma_a \eta_v} - e^{-\gamma_b \eta_v}) = T_f, \quad (39)$$

$$\delta - \frac{\Omega T_v \xi R_f}{U q_v (\gamma_a - \gamma_b)} \left(\frac{e^{-\gamma_a \eta_v} - 1}{\gamma_a} - \frac{e^{-\gamma_b \eta_v} - 1}{\gamma_b} \right) = \frac{\Omega (T_f - T_v)}{U q_v (\mu_a - \mu_b)} \left(\frac{e^{-\chi_a \eta_c} - 1}{\chi_a^2} - \frac{e^{-\chi_b \eta_c} - 1}{\chi_b^2} \right), \quad (40)$$

where $Q(T_f)$ is the normalized chemical heat release at the flame front,

$$Q(T_f) = [\sigma + (1 - \sigma) T_f]^2 \exp \left[\frac{Z}{2} \left(\frac{T_f - 1}{\sigma + (1 - \sigma) T_f} \right) \right]. \quad (41)$$

If the reactants around the flame front R_f are homogeneous, then the correlation is

$$\frac{\xi T_v}{\gamma_a - \gamma_b} [\gamma_a \theta_a - \gamma_b \theta_b] e^{\xi \eta_c} = Q(T_f), \quad (42)$$

$$-I'_1(0) \left[\mathcal{H}(\eta_v, \eta_c) - \frac{I'_2(\eta_c)}{I'_1(\eta_c)} \right] / Le = Q(T_f), \quad (43)$$

$$T_v + \frac{T_v}{\gamma_a - \gamma_b} (\gamma_a \theta_a - \gamma_b \theta_b) (1 - e^{\xi \eta_c}) - \frac{\xi T_v}{\gamma_a - \gamma_b} (\theta_a - \theta_b) = T_f, \quad (44)$$

$$\frac{\Omega \xi T_v}{U q_v (\gamma_b - \gamma_a)} \left[\frac{1 - e^{\gamma_a(\eta_c - \eta_v)}}{\gamma_a} - \frac{1 - e^{\gamma_b(\eta_c - \eta_v)}}{\gamma_b} \right] = \delta. \quad (45)$$

The implications of the four equations in the correlations for heterogeneous and homogeneous flames are as follows:

- (a) The first equation [Eqs. (37) and (41)] indicates that heat absorbed by the gaseous mixture and droplet is equal to the heat produced by reaction.

- (b) The second equation [Eqs. (38) and (42)] means the heat supplied by the initial fuel vapor and heat supplied by vaporized fuel vapor is equal to the heat from chemical reaction.
- (c) The third equation [Eqs. (39) and (43)] is the continuity of the gaseous temperature at the flame front for the pre-flame evaporation zone (zone 2).
- (d) For the last equation, Eq. (40) means the continuity of the droplet loading at the flame front for the pre- and post-flame evaporation zones for heterogeneous flames. Meanwhile, Eq. (45) indicates the continuity of the droplet loading at the evaporation completion front [$Y_d(\eta_c) = 0$] for the pre-flame evaporation zone in homogeneous flames.

Furthermore, the analytical solutions and correlations corresponding to the two critical scenarios mentioned in Sec. II C, i.e., $\eta_c = 0$ and $\eta_c = -R_f$, will be provided in the [supplementary material](#). Besides, the results for the homogeneous flame from the current model can recover the solutions for the gaseous flame³⁵ in the limits of $\delta \rightarrow 0$, $\Omega \rightarrow 0$, and $R_f \rightarrow +\infty$, which are also presented in the [supplementary material](#).

IV. RESULTS AND DISCUSSION

With the correlations in Sec. III B, spherical flame propagation in pre-vaporized liquid fuel sprays will be studied. In Secs. IV A–IV E, both heterogeneous (without droplet burning, $\alpha = 0$) and homogeneous flames will be discussed. In Sec. IV F, the influence of droplet burning behind the heterogeneous flame ($\alpha = 1$) will be studied. The normalized latent heat of vaporization q_v considered is 0.4 and 1.2, representing typical hydrocarbon fuels with low and high latent heat (e.g., heptane and methanol), respectively.⁴⁸

A. Spherical flame propagation

The effects of droplet properties (mass loading δ , evaporative heat exchange coefficient Ω , and latent heat of vaporization q_v) on spherical flame propagation will be first investigated. The Lewis number is fixed to be $Le = 1$. Figure 2(a) shows the change in flame propagation speed with various droplet mass loadings. Here, $\Omega = 0.2$ and $q_v = 0.4$. It is seen that for all the mass loadings, the flame propagation speed rapidly increases with the flame radius due to enhanced diffusive flux, eventually approaching those

of the un-stretched planar flames ($R_f \rightarrow +\infty$).³⁵ Furthermore, for the same flame radius, propagation speed is higher than that of the gaseous flame and increases with the initial droplet loading. This is because more liquid fuels are vaporized into the gas phase, rendering the composition closer to the stoichiometry. It is also found that when droplet loading is small (e.g., $\delta = 0.01$ and 0.1), the reactants around propagating spherical flame front are homogeneous. However, with $\delta \geq 0.2$, they are heterogeneous and composed of fuel vapor and droplets. This is because bigger δ corresponds to higher droplet concentration. Interestingly, for $\delta = 0.15$, the flame first propagates in homogeneous reactants, but at $R_f \approx 18.9$ (marked with circle C), the droplets in the unburned zone cross the moving flame front, and the spray flame transitions to heterogeneous combustion.

The propagation speed of spherical flames with various evaporative heat exchange coefficients Ω is presented in Fig. 2(b). Here, $\delta = 0.2$ and $q_v = 0.4$. In general, the flame propagation speed is higher with larger Ω when the loading is fixed. This is justifiable since larger Ω means the faster droplet evaporation rate. However, this tendency becomes weak when $\Omega = 0.35$ and 0.4 . For $\Omega = 0.35$ in Fig. 2(b), transition between homogeneous and heterogeneous flames at $R_f \approx 26$ (circle D) are observed, similar to the case with $\delta = 0.15$ in Fig. 2(a).

Figures 3(a) and 3(b) show two flame structures with $\delta = 0.1$ and 0.3 [A and B in Fig. 2(a)], respectively. Their flame radii are $R_f = 100$. Note that Fig. 3(a) shows a homogeneous flame, while Fig. 3(b) shows a heterogeneous one. In Fig. 3(a), the droplets are fully vaporized (i.e., $Y_d \rightarrow 0$) slightly before the flame front ($\eta_c = 0.246$). The extra fuel addition from droplet evaporation increases the overall fuel concentration in the gaseous mixture, leading to higher temperature in the post-flame zone compared to that ($=1$) of droplet-free flames. Meanwhile, due to no droplet evaporation in the post-flame zone ($\eta < 0$), the local temperature is uniform.

The heterogeneous flame structure in Fig. 3(b) is different from that of homogeneous one. First, finite fuel concentration can be found in the post-flame zone since evaporation of the penetrated droplets occurs and burning is not considered ($\alpha = 0$). The presence of fuel vapor behind the flame is also revealed by Greenberg and Kalma⁵² from spherical flame with less volatile liquid fuel sprays. Part of them contribute toward the spray flame through back diffusion from the post-flame zone to the flame front, which is also observed from the simulations and experiments of the

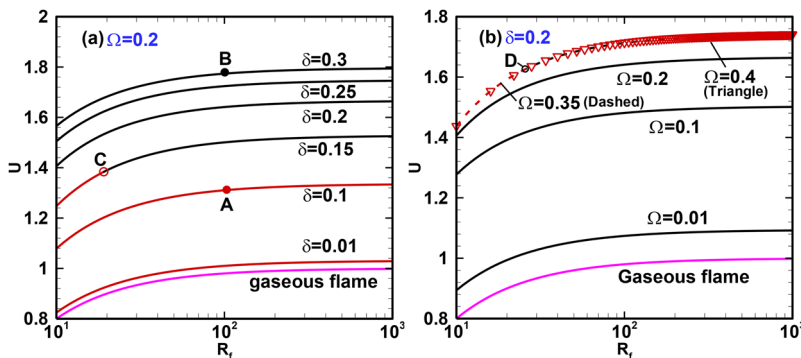


FIG. 2. Changes in flame propagation speed with flame radius for different (a) droplet mass loadings and (b) evaporative heat exchange coefficients. $Le = 1$ and $q_v = 0.4$. Red line and triangles: homogeneous; black line: heterogeneous.

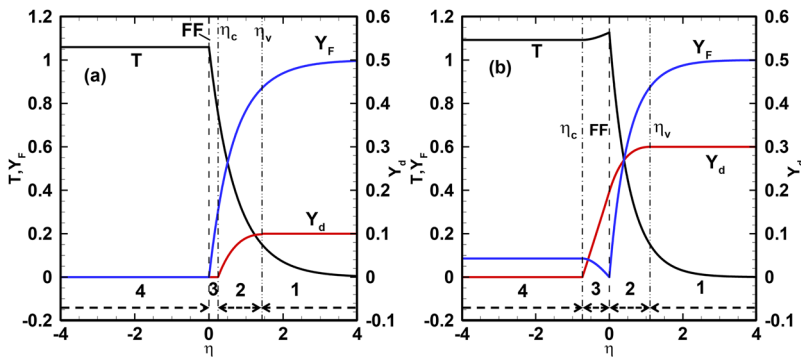


FIG. 3. Spatial distributions of temperature, fuel mass fraction, and droplet mass loading for $R_f = 100$ when (a) $\delta = 0.1$ and (b) $\delta = 0.3$. Numbers indicate the flame and droplet zones. FF: flame front ($\eta = 0$).

propagating flame in fuel mists.^{15,21,53} The post-flame evaporation and its evolving interaction with the leading stretch flame front are of high relevance to practical spray combustion but has not been included in previous theoretical analysis.^{26,27} Moreover, there are still residual fuel vapors beyond the evaporation zone in the burned area, i.e., $\eta < \eta_c$. This is different from the results in the homogeneous flame, and the kinetic effects of the heterogeneous flame arise from both pre- and post-flame evaporation zones (further interpreted in Sec. IV C). Second, the gas temperature in the post-flame zone gradually decreases from the flame front in the post-flame evaporation zone. Heat conduction in this zone (i.e., $\eta_c < \eta < 0$) would also weaken the flame reactivity due to the considerable temperature gradient near the flame front. This is also reported from the results of spherical premixed flame with water mists.²⁹

The latent heat of vaporization considered in Figs. 2 and 3 is $q_v = 0.4$. However, different liquid fuels may be used in practical combustion systems, and they have different latent heat. Figure 4 shows flame propagation speed as a function of flame radius when $q_v = 1.2$. Four droplet mass loadings are considered in Fig. 4(a), i.e., $\delta = 0.01, 0.1, 0.3, 0.5$, and 0.7 . The evaporative heat exchange coefficient Ω is assumed to be 0.0775 . For $\delta \leq 0.5$, the single-valued flame speed monotonically increases when the spherical flame propagates outwardly. They are called normal flames. In addition, the flame propagation speed is consistently smaller than that of a gaseous flame. Meanwhile, for normal flames, the propagation speed decreases with droplet loading. Nevertheless, this trend is not pronounced when δ is beyond 0.3 .

For $\delta = 0.7$ in Fig. 4(a), flame bifurcation occurs. Besides the normal flame branch, a C-shaped branch is present when $R_f > 74$, with upper and lower solutions being unstable and stable flames. Therefore, three solutions are present when the flame radius exceeds a critical value. This is also observed in the previous studies on two-phase spherical flames laden with water mists.^{29,32} These three flames, respectively, correspond to the stable normal flame, unstable flame, and stable weak flame. For normal flames, their behaviors of propagation speed, evaporation completion, and onset fronts are similar to the results with smaller δ . For the weak flame, the propagation speed decreases with flame radius and is much lower than the normal flame.

The propagation speeds of spherical spray flame subject to various evaporation heat exchange coefficients are shown in Fig. 4(b). Here, fixed $\delta = 0.7$ is considered. For small Ω (e.g., 0.06), the heat transfer due to droplet vaporization is slow, and the normal spray flames propagate outwardly. At some median values, i.e., $\Omega = 0.0775$ and 0.08 , flame bifurcation occurs, similar to that in Fig. 4(a). Both normal and weak flames exist in Fig. 4(b) when $\Omega = 0.0775$ and 0.08 . Meanwhile, increasing Ω would sustain the weak flame in a smaller flame radius. However, if Ω is even higher (0.1 or 0.3), the spray flame can only propagate in the weak flame mode due to fast droplet evaporation rate and strong heat absorption. Meanwhile, the large Ω would render the mixture heterogeneous around the flame front, which is also seen from Fig. 2(b).

One interesting phenomenon worth further discussion is that for $\Omega = 0.06$ in Fig. 4(b), the evaporation rate is so slow that the

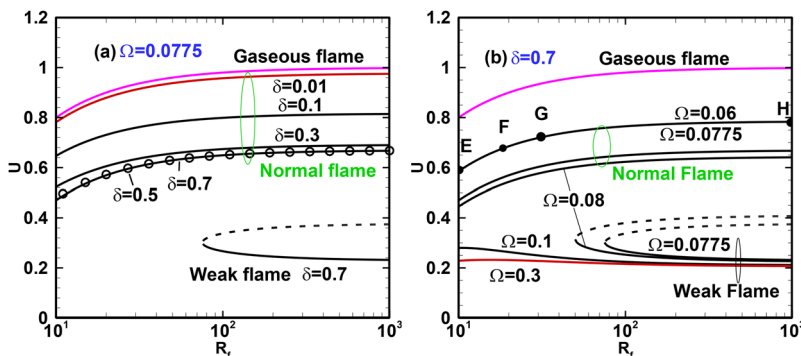


FIG. 4. Changes in flame propagation speed with flame radius for different (a) droplet mass loadings and (b) evaporative heat exchange coefficients. $Le = 1$ and $q_v = 1.2$. Symbol and red line: homogeneous; black line: heterogeneous. Dotted line: $\eta_c = -R_f$.

droplets are distributed in the full post-flame zone when the flame radius is small (line EF). At a critical flame radius ($R_f = 19.9$, point F), the droplets at the center ($r = 0$ or $\eta = -R_f$) are just fully vaporized. When the flame further grows, the droplet-free area centering at $r = 0$ expands, and hence, only part of the post-flame zone still has evaporating fuel droplets (line FH). To reveal this phenomenon, the flame structures at E, F, and G are presented in Fig. 5. When $R_f = 10$ (point E), considerable gradients exist for temperature, fuel mass fraction, and droplet loading in zone 3 as evaporating droplets are distributed in the entire burned area and the loading at the spherical center, δ_r , is greater than zero [solid circle in Fig. 5(a)]. This would lead to significant heat and mass transfer between the flame front and the burned area. When $R_f = 19.9$ (point F), the droplets around the spherical center are just fully gasified. Thus, the droplet loading at $r = 0$ is $\delta_r = 0$ [circle in Fig. 5(b)]. Here, the evaporation completion front lies at the spherical center, as the limiting case with $\eta_c = -R_f$, mentioned in Sec. II C. For these two scenarios, only three zones exist. For point G ($R_f = 30$), the droplets are dispersed in part of the post-flame zone. Thus, the evaporation completion front [circle in Fig. 5(c)] is deviated from the spherical center and moves concurrently with the leading flame front. Its structure is qualitatively like that in Fig. 3(b), despite the lower temperature in the post-flame zone due to larger latent heat. This corroborates the capacity of our theoretical model in predicting the fuel droplet dynamics in a propagating spray flame.

B. Fuel droplet distribution

The homogeneous and heterogeneous spherical spray flames discussed above are characterized by evolving droplet distributions

when they propagate outwardly, which can be further quantified with evaporation onset and completion locations (η_v and η_c). Figures 6(a) and 6(b) shows the evolutions of the two characteristic locations with various mass loadings δ and heat exchange coefficients Ω , respectively. Their corresponding flame propagation speeds are shown in Figs. 2(a) and 2(b), respectively. Droplet evaporation always starts before the flame sweeps, parameterized by $\eta_v > 0$ in both figures. In Fig. 6(a), for fixed Ω , when the droplet loading is increased, the droplets start to vaporize closer to the flame front. This is because larger δ leads to higher flame temperature and hence less spread temperature in the pre-flame zone.²⁹

The variations of evaporation completion location η_c are more complicated. When the loading δ is low (e.g., 0.01 and 0.1), the flame always propagates in a homogeneous mixture with fuel vapor only. Nevertheless, when δ is high (0.2–0.3), the reactants around the flame front are heterogeneous with fuel vapor and droplets. In particular, when δ is 0.15, the liquid droplets are completely vaporized when the flame radius is small but slightly penetrate into the post-flame zone as the spherical flame expands. Therefore, evolution from homogeneous flame to heterogeneous flame occurs at point C in Fig. 6(a). This is reasonable since it takes longer time for the fuel droplet sprays to complete evaporation when δ is large. This phenomenon is also observed by de Oliveira and Mastorakos using simultaneous OH* chemiluminescence and OH-PLIF imaging of spray jet A flames,¹⁵ and it is found that the local microscopic flame topology may be modulated by the encroaching droplets, which significantly affect the local mass and heat transfer near the flame front.

In Fig. 6(b), for fixed $\delta = 0.2$, change in Ω has a limited effect on evaporation onset locations η_v . Moreover, higher Ω makes the

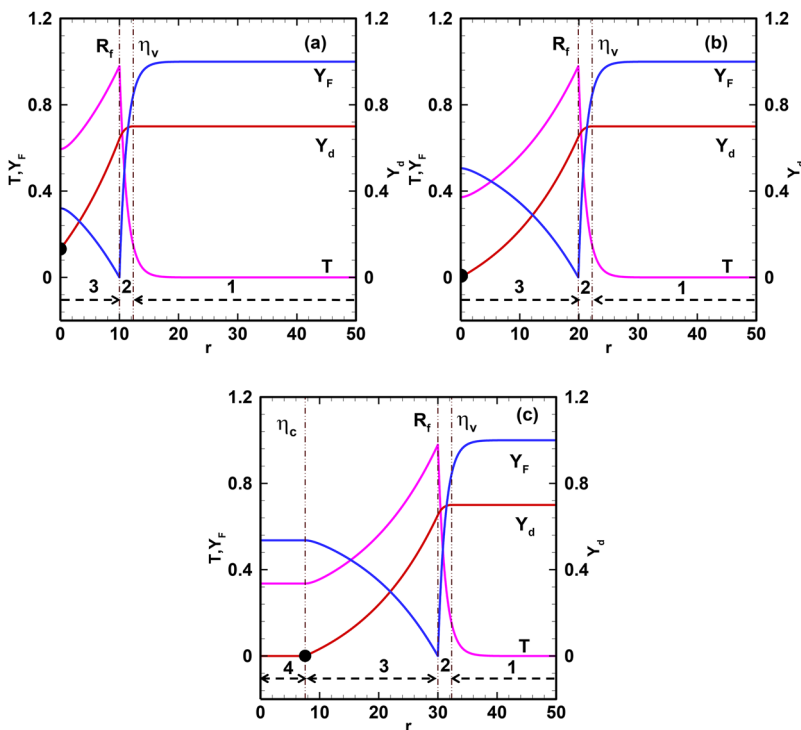


FIG. 5. Spatial distributions of temperature, fuel mass fraction, and droplet mass loading for (a) $R_f = 10$, (b) $R_f = 19.9$, and (c) $R_f = 30$. They correspond to the circles E, F, and G in Fig. 4, respectively. Numbers indicate the flame and droplet zones.

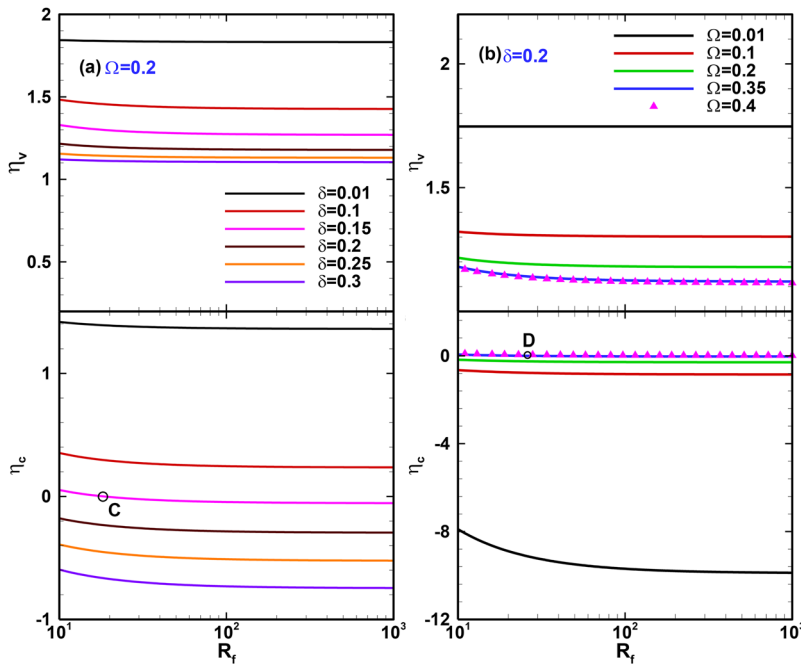


FIG. 6. Changes in evaporation onset and completion locations with flame radius for different (a) droplet mass loadings and (b) evaporative heat exchange coefficients. $q_v = 0.4$.

evaporation completion front closer to the flame front ($\eta = 0$). Note that for $\Omega = 0.35$, the flame experiences a transition from the homogeneous to heterogeneous flame at $R_f \approx 26$ (marked with an open circle D). It is also found from Fig. 6(b) that the thickness of the droplet evaporation zone, i.e., $|\eta_c - \eta_v|$, increases with decreased Ω . This is due to the slower evaporation rate corresponding to smaller Ω .

The various distributions of liquid droplets may have different thermal (evaporative cooling) and kinetic (fuel vapor addition) contributions toward the spherical spray flame. The evaporative cooling effects can be quantified by normalized evaporation heat loss H .^{29,35} In the unburned and burned zones of a heterogeneous flame, H is, respectively, calculated as

$$H_{ub,HT} = \Omega \int_0^{\eta_v} [T_2(\xi) - T_v](\xi + R_f)^2 d\xi / \left(R_f^2 \frac{dT}{d\eta} \Big|_{-} - R_f^2 \frac{dT}{d\eta} \Big|_{+} \right), \quad (46)$$

$$H_{b,HT} = \Omega \int_{\eta_c}^0 [T_3(\xi) - T_v](\xi + R_f)^2 d\xi / \left(R_f^2 \frac{dT}{d\eta} \Big|_{-} - R_f^2 \frac{dT}{d\eta} \Big|_{+} \right). \quad (47)$$

For a homogeneous flame, they are

$$H_{ub,HM} = \Omega \int_{\eta_c}^{\eta_v} [T_2(\xi) - T_v](\xi + R_f)^2 d\xi / \left(R_f^2 \frac{dT}{d\eta} \Big|_{-} - R_f^2 \frac{dT}{d\eta} \Big|_{+} \right), \quad (48)$$

$$H_{b,HM} = 0. \quad (49)$$

The subscripts “ub” and “b” denote evaporative heat loss from unburned and burned zones, respectively, whereas “HM” and “HT”

denote homogeneous and heterogeneous flames, respectively. The denominator, , is the combustion heat release. Equation (49) is valid since there are no droplets in the burned zone of homogeneous flames. The total evaporation heat loss is $H_{all} = H_b + H_{ub}$.

The fuel addition from droplet evaporation can be parameterized by fuel vapor yield f .²⁷ In the pre-flame evaporation zone, f_{ub} is

$$f_{ub} = Y_d(\eta_v) - Y_d(0). \quad (50)$$

For a heterogeneous flame, in the post-flame zone, f_b is

$$f_b = Y_d(0) - Y_d(\eta_c). \quad (51)$$

The total fuel vapor yield is $f_{all} = f_{ub} + f_b$. Note that for a homogeneous flame, f_b is zero since no evaporation occurs behind the flame front. Accordingly, $f_{all} = f_{ub}$ holds.

Figure 7(a) shows the normalized evaporative heat loss for three flames with different δ and Ω in Fig. 6. For the homogeneous flames, the evaporation induced heat transfer only occurs in the pre-flame zone, and $H_{ub,HM}$ almost remains constant when the flame expands. Meanwhile, for the heterogeneous flame, $H_{ub,HT}$ ($H_{b,HT}$) decreases (increases) with the flame radius, which leads to monotonically (but subtly) increased H_{all} . Besides, the higher δ , the higher H_{all} . Meanwhile, for fixed droplet loading, e.g., $\delta = 0.2$, H_{all} is almost independent on Ω .

Figure 7(b) shows the corresponding fuel vapor yield. For the homogeneous flames, the fuel vapor from droplet evaporation only exists in the pre-flame zone. For the heterogeneous flame, the fuel vapor exists in both pre- and post-flame zone. Note that the total fuel vapor yield f_{all} is the same as the droplet loading δ for all the shown flames due to the complete droplet evaporation in the domain.

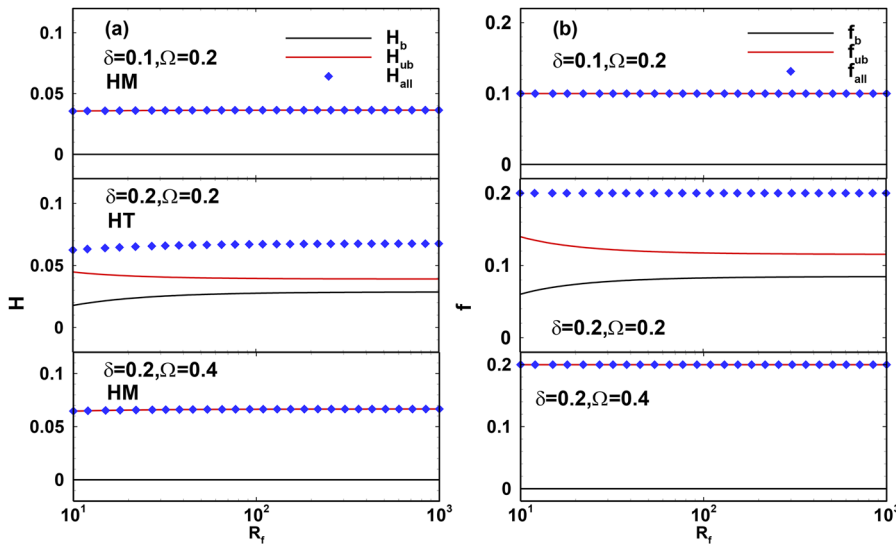


FIG. 7. Changes in (a) evaporation heat loss and (b) fuel vapor yield with flame radius.

With increased δ or decreased Ω , f_b increases. This is because more droplets cross the flame front and finish evaporation there.

The influences of liquid fuel latent heat of vaporization on droplet distribution in a propagating flame are examined in Fig. 8(a), which shows the evaporation onset and completion locations as functions of flame radius R_f . The latent heat q_v is 1.2, higher than that in Figs. 6 and 7. The evaporative heat loss coefficient Ω is 0.0775, and the flame propagation speed has been studied in Fig. 4(a). For $\delta \leq 0.3$, the flame speed acceleration leads to more droplets behind the flame front, and the evaporation completion front penetrates further in the post-flame zone when the flame propagates outwardly.

Meanwhile, the evaporation onset front deviates from the flame front when δ is increased. For $\delta = 0.7$, bifurcation of droplet evaporation characteristic locations is also observed, the same as the flame bifurcation in Fig. 4(a). For the normal flame, the behaviors of evaporation completion and onset fronts are like those with smaller δ . However, for the weak flame, the evaporation completion front moves closer to the flame front since the droplet evaporation starts earlier when the flame front moves outwardly.

For fixed droplet loading $\delta = 0.7$ in Fig. 8(b), with decreased Ω , the trends for both normal flame and weak flame are similar to those with increased δ in Fig. 8(a). However, for the normal flame with

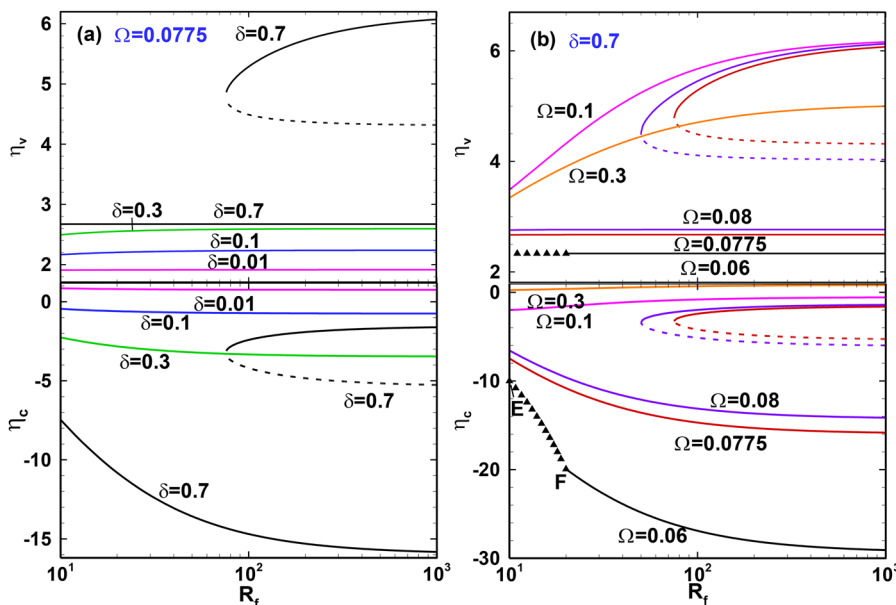


FIG. 8. Changes in evaporation onset and completion locations with flame radius for different (a) droplet mass loadings and (b) evaporative heat exchange coefficients. $Le = 1$ and $q_v = 1.2$. Dashed line: unstable solution; triangle: $\eta_c = -R_f$.

$\Omega = 0.06$, the fuel droplets are distributed in the entire post-flame zone at the early stage of flame propagation, which corresponds to the critical heterogeneous flames with $\eta_c = -R_f$ (triangles between E and F). This has been discussed in Figs. 4(b) and 5.

Figure 9(a) shows the normalized evaporative heat loss for the three flames selected from Fig. 8. It is found that when $\delta = 0.1$, variations in H_{all} are limited when the flame propagates. Meanwhile, H_b and H_{ub} are comparable. When $\delta = 0.7$, for the normal flames with $\Omega = 0.06$ and 0.0775 , H_{all} and H_b mainly contributes toward H_{all} , both of which gradually increase when the flame radius increases, while H_{ub} is relatively small. This is because more droplets vaporize behind the flame front. For the weak flame with $\Omega = 0.0775$, H_{all} does not change with the flame radius, with close contributions from H_b and H_{ub} .

Figure 9(b) shows the fuel vapor yield corresponding to the same heterogeneous flames in Fig. 9(a). The relations between f_b and f_{ub} are similar to those between H_b and H_{ub} indicated in Fig. 9(a). $f_{ub} = \delta$ holds if all the droplets are vaporized. However, for $\delta = 0.7$ and $\Omega = 0.06$, when the flame radius is small, droplets exist in the full domain, as mentioned in Figs. 5 and 8. Therefore, under this condition, f_b and f_{all} gradually increase with the droplet loading at the spherical center δ_r decreasing to zero [see Fig. 9(b)].

C. Diffusive fluxes in homogeneous and heterogeneous flames

To elucidate the respective influences of thermal and kinetic effects, diffusive heat and mass fluxes (Q_h and Q_m) of homogeneous

and heterogeneous flames are calculated as

$$Q_h = -(\eta + R_f)^2 \frac{dT}{d\eta}, \tag{52}$$

$$Q_m = -\frac{(\eta + R_f)^2}{Le} \frac{dY_F}{d\eta}. \tag{53}$$

Typical flames with Lewis number $Le = 1$ and flame radius $R_f = 100$ are selected for further analysis in Figs. 10 and 11. Figure 10 shows the heat and mass fluxes of homogeneous ($\delta = 0.1$) and heterogeneous flames ($\delta = 0.2$) with $q_v = 0.4$. They correspond to flames A and B in Fig. 2(a), respectively. Gaseous (no droplets, only pre-vaporized fuel) flame is also added for comparison. For gaseous and homogeneous spray flames, due to the uniform distributions of temperature and fuel mass fraction in the post-flame zone [see Fig. 3(a)], the heat and mass fluxes are zero. Conversely, heat conduction and fuel species diffusion only occur in the pre-flame zone.

For the heterogeneous spray flame, the fluxes in the pre-flame zone show similar behaviors to the homogeneous flame. However, due to the droplet evaporation in the post-flame zone, the fuel vapor is transported to the flame front, while heat released by the chemical reactions at the flame front is diffused into the post-flame evaporation zone to compensate the local evaporation heat loss. The magnitude of mass flux $|Q_m|$ is higher than that of heat flux $|Q_h|$, in spite of the same diffusion length. Moreover, both thermal and mass diffusion in homogeneous and heterogeneous flames are enhanced compared to the gaseous flame, evidenced by the higher flux magnitudes. This leads to stronger spray flames with higher propagation

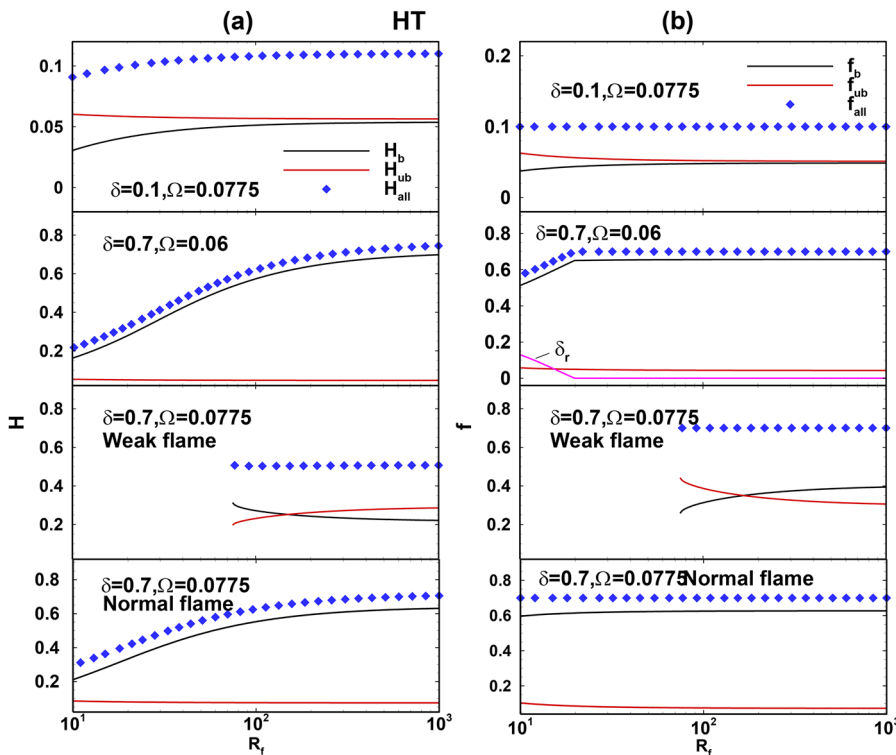


FIG. 9. Changes in (a) evaporation heat loss and (b) fuel vapor yield with flame radius.

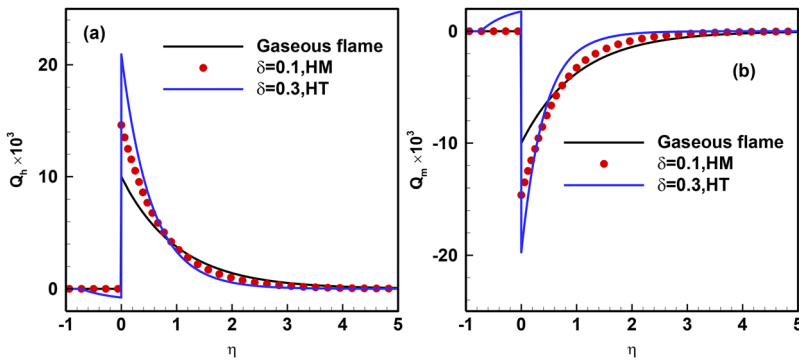


FIG. 10. Distributions of (a) heat flux and (b) mass flux. $R_f = 100$, $q_v = 0.4$, and $\Omega = 0.2$. The flame front lies at $\eta_f = 0$.

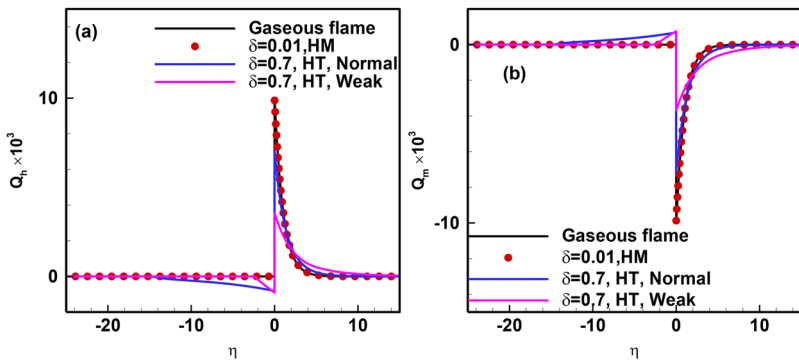


FIG. 11. Distributions of (a) heat flux and (b) mass flux. $R_f = 100$, $q_v = 1.2$, and $\Omega = 0.0775$. The flame front lies at $\eta_f = 0$.

speeds. In addition, near the flame front, $|Q_h|$ and $|Q_m|$ in heterogeneous flames are larger than the counterparts of homogeneous flames due to stronger reactivity and hence higher gradient of T and Y_F in the former.

The counterpart results with higher latent heat, i.e., $q_v = 1.2$, are presented in Fig. 11. They correspond to the flames with same parameters in Figs. 4(a) and 8(a). The trends for homogeneous and heterogeneous flames are similar to those in Fig. 10. For small δ like 0.01, the fuel droplet evaporation effect on the flame is limited, and both fluxes are similar to those of the gaseous flame. However, due to the weakening effect from larger q_v , with increased δ , $|Q_h|$ and $|Q_m|$ decrease to a lower level compared to the gaseous flame.

Furthermore, for $\delta = 0.7$, $|Q_h|$ and $|Q_m|$ of the weak flame are much smaller than those of the normal flame. Due to the low reactivity of the weak flame, its structure is more distributed with lower gradients of T and Y_F . In the meanwhile, in the burned zones of the normal and weak flames, $|Q_m|$ is slightly larger than $|Q_h|$.

D. Lewis number effect

Up to this point, the Lewis number is assumed to be $Le = 1$. Figure 12(a) shows the flame propagation speed U as a function of flame radius R_f when $Le = 0.8, 1.0$, and 1.2 . Here, $q_v = 0.4$ and $\Omega = 0.2$ are considered. It is seen that flame propagation speeds of both

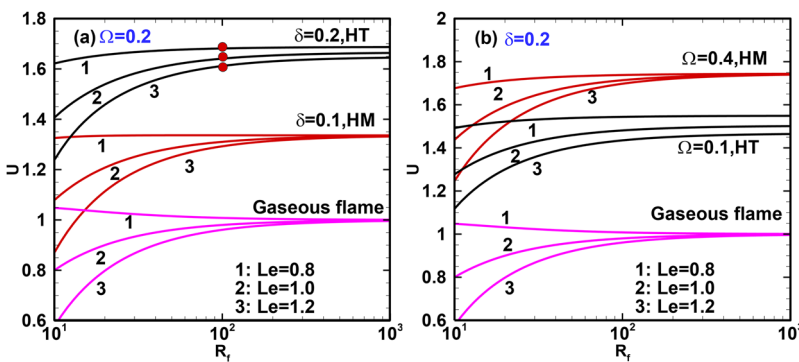


FIG. 12. Changes in flame propagation speed with flame radius for different Lewis numbers when (a) $\Omega = 0.2$ and (b) $\delta = 0.2$.

homogeneous and heterogeneous spherical flames are dependent on the Lewis number. Generally, with each Lewis number, U increases with δ because of the spray enrichment effects.⁵⁴ Furthermore, U decreases with the Lewis number when R_f is small or intermediate due to the flame stretch effects.⁵⁵ This is true for both homogeneous and heterogeneous flames. In particular, when $Le = 0.8$, U monotonically decreases with R_f for homogeneous and gaseous flames with $\delta = 0.1$ because of the continuously reduced enhancement effects from the positive stretch. However, when δ is further increased to 0.2, a monotonic increase in U with R_f is observed. This implies that the fuel vapor addition dominates the foregoing stretch effects.⁵⁴ For relatively large R_f (e.g., 10^3), the propagation speed for the homogeneous flame is independent on Le , similar to the gaseous flame. However, U for the heterogeneous flame in large R_f is appreciably affected by Le due to the additional transport phenomenon related to droplet evaporation behind the flame front. This is consistent with the recent finding of planar spray heterogeneous flames with fuel mists.²⁸

Figure 12(b) shows the Lewis number effects on the flame propagation speed when the evaporation heat exchange coefficient Ω varies. For homogeneous and heterogeneous flames, their tendencies for U variations with Le are generally similar to the counterpart flames in Fig. 12(a). When $Le = 0.8$, the kinetic contributions from fuel sprays exceed the flame stretch effects, which makes U monotonically increase with R_f . This is observable for $\Omega = 0.1$ and 0.4 and different from the gaseous flame results.

Figures 13(a) and 13(b), respectively, show the heat and mass fluxes in pre- and post-flame zones of heterogeneous flames (marked with circles in Fig. 12) with $Le = 0.8, 1.0$, and 1.2. It is seen that in both zones, variation in the Lewis number only affects the mass

fluxes. Specifically, lower Le increases the mass flux magnitude and hence enhances the flame reactivity, characterized by the higher propagation speed shown in Fig. 12(a).

E. Markstein length

The effects of stretch rate on homogeneous and heterogeneous spherical spray flames will be further studied in this section. For weakly stretched spherical flames ($R_f \gg 1$ or $K \ll 1$), the following relation holds between flame propagation speed U and stretch rate K :^{34,55}

$$U = U^0 - L \cdot K, \tag{54}$$

where U^0 is the flame speed at the zero stretch rate. For spherical flames, stretch rate K can be derived from $K = 2U/R_f$. Specifically, for gaseous and homogeneous spherical flames, the flame stretch rate K is positive. Interestingly, for heterogeneous flames, due to the concurrent transport before and after the propagating flame front, K is, respectively, positive and negative for them. Therefore, their individual effects, together with the Lewis number, on flame propagation speeds would be opposite due to the reversed flame surface curvature and therefore competitive. For instance, if $Le < 1$, the positive K (for the unburned area) accelerates the flame, whereas the negative K (for the burned area) decelerates it.⁵⁵ Therefore, Eq. (54) measures the gross response of the heterogeneous flame propagation speed to the stretch rate. Nonetheless, from Figs. 10, 11, and 13, it is seen that the transport in the burned area is comparatively lower, and therefore, the mass and thermal diffusion in the fresh gas still dominate. Figure 14 shows the U - K curves corresponding to the results in Fig. 12. For outwardly propagating spherical flames, the

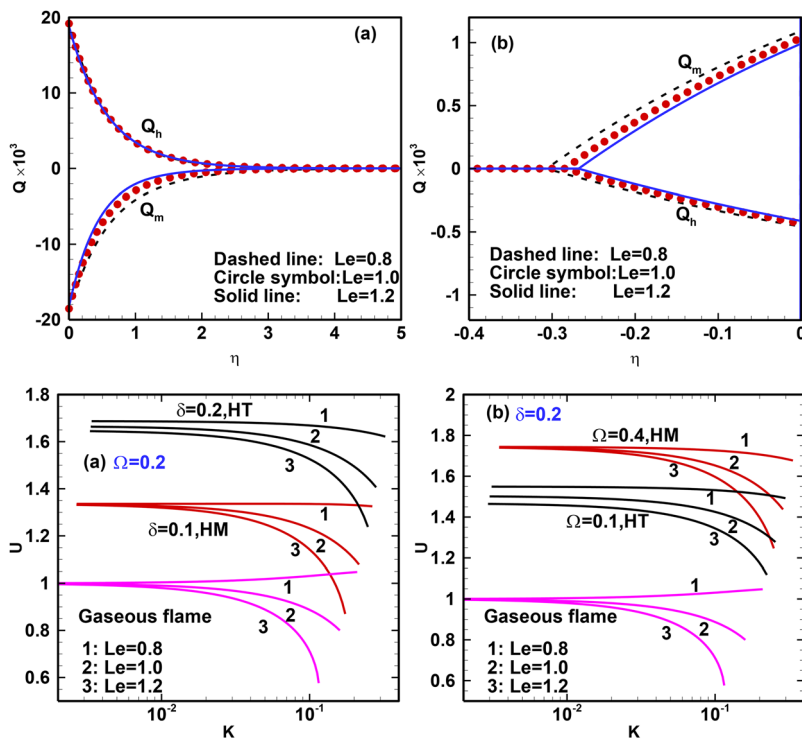


FIG. 13. Distributions of heat and mass fluxes for different Lewis numbers in (a) pre- and (b) post-flame zones. $q_v = 0.4$ and $R_f = 100$. The flame front lies at $\eta = 0$.

FIG. 14. Changes in flame propagation speed with stretch rate for different Lewis numbers when (a) $\Omega = 0.2$ and (b) $\delta = 0.2$.

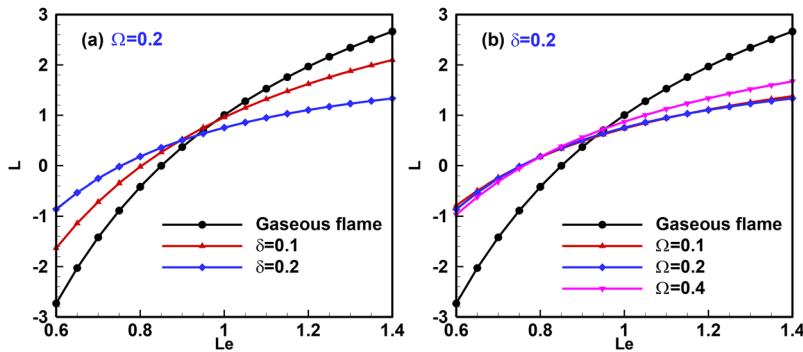


FIG. 15. Markstein length vs Lewis number when (a) $\Omega = 0.2$ and (b) $\delta = 0.2$.

larger the flame radius, the lower the stretch rate. Figure 14 indicates that a linear relation exists between U and K when K is low,^{27,56} and therefore, the Markstein length L (slope of the U - K curve) can be calculated with Eq. (54).

Figure 15 shows the Markstein length with various Lewis numbers in the flames of Figs. 12 and 14. Generally, the Markstein length L is considerably affected by droplet mass loading and evaporation heat exchange coefficient when the Lewis number deviates from unity. For $Le < 1$ ($Le > 1$), L is negative (positive), indicating that the flame propagation speed is enhanced (decreased) relative to U^0 . The norms of L in spray flames are reduced compared to gaseous flames with the same Le , which implies that the degrees of the enhancement or reduction of spray flame propagation are weakened. In addition, this extent is enhanced with the droplet loading δ when Ω is fixed, as shown in Fig. 15(a). However, it is shown from Fig. 15(b) that for fixed δ , the sensitivity of the Markstein length to Ω is less pronounced.

F. Droplet burning behind a heterogeneous flame

In Secs. IV A–IV E, for heterogeneous flames, droplet burning behind the flame front is not considered. To examine this effect, two heterogeneous flames ($\delta = 0.15$ and 0.3) from Fig. 2(a) are recalculated with $\alpha = 1$ in this section. The corresponding U - R_f curves are shown in Fig. 16(a). Apparently, for $\delta = 0.3$, the heterogeneous flame propagation speed is higher when droplet burning is included. This is also reported by Han and Chen.²⁷ The structure of the

heterogeneous flame with droplet burning [B' in Fig. 16(a), $R_f = 100$] is shown in Fig. 3(b). For comparison, the results without droplet burning [B in Fig. 16(a), also shown in Fig. 3(b)] are also added. First, due to post-flame droplet burning, Y_F in the post-flame zone is zero since $\tilde{\omega} = \alpha\tilde{\omega}_v$ in Eq. (2). Moreover, the heat release of droplet burning in the post-flame zone leads to higher temperature compared to the same condition when post-flame burning is not considered. Meanwhile, different from flame B, a negative temperature gradient exists behind the reaction front in flame B' , resulting in higher propagation speed unveiled in Fig. 16(a).

Moreover, in Fig. 16(a), for $\delta = 0.15$, a transition from the homogeneous to heterogeneous flame occurs at C for both $\alpha = 0$ and 1. Note that their transition point is the same. This is reasonable since droplet burning does not affect the results of homogeneous one. Nonetheless, when $\alpha = 1$, sudden flame acceleration is observable from increased dU/dR_f across C (not shown here), leading to slightly higher U of heterogeneous flames with droplet burning.

Figure 17 shows the influences of droplet burning on Markstein length of heterogeneous flames with different Lewis numbers and droplet mass loadings. It is found that when $\delta = 0.3$, droplet burning in the post-flame zone negligibly affects the Markstein length. However, when δ is reduced to 0.15, the magnitude of Markstein length is higher when $\alpha = 1$, indicating that flame stretch has stronger effects on the propagation speeds when droplet burning is included. For heterogeneous flames with smaller droplet loading, the evaporation completion location is closer to the flame front

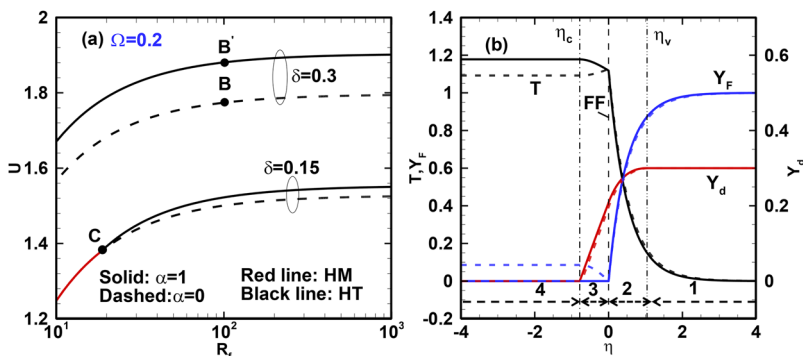


FIG. 16. (a) Changes in heterogeneous flame propagation speed with flame radius and (b) spatial distributions of temperature, fuel mass fraction, and droplet mass loading for points B' (solid) and B (dashed). $Le = 1$.

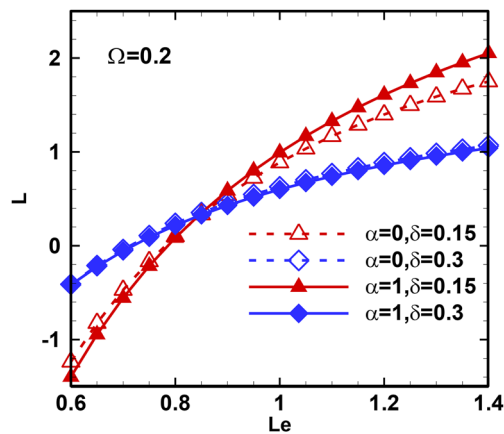


FIG. 17. Effects of droplet burning on Markstein length with various Lewis numbers and droplet mass loadings.

[see Fig. 6(a)], and hence, the burning droplets would more appreciably affect the leading flame front through modulating the local heat and mass transfer.

V. CONCLUSION

Propagation of weakly stretched premixed spray flames in localized homogeneous and heterogeneous reactants is investigated in this work. A general theory based on one-dimensional spherical spray flames with evaporating fuel droplets is developed, and correlations are derived to describe flame propagation speed, flame temperature, droplet evaporation onset, and completion locations. The theory enables the analysis on the influences of liquid fuel and gaseous mixture properties on propagation of spherical spray flames. The main conclusions are listed as follows:

1. The flame propagation speed is enhanced with increased droplet mass loading and/or evaporation heat exchange coefficient (or evaporation rate). Opposite tendencies are observed when the latent heat is high due to strong evaporation heat loss. For heterogeneous flames, there exist gradients for fuel vapor and gaseous temperature in the post-flame zone when post-flame burning is not considered. For large latent heat, when the droplet loading is large, flame bifurcation phenomenon occurs.
2. The evaporation completion location relies on the droplet properties. For large droplet loading or small heat exchange coefficient, the reactants around the flame front are heterogeneous. In some extreme condition, the droplets are distributed in the entire post-flame zone. Besides, the spray flame experiences a transition from localized homogeneous to heterogeneous conditions in intermediate droplet loading or heat exchange coefficient. These dynamic droplet behaviors can be predicted with the developed theory.
3. Heat and mass diffusion for both heterogeneous and homogeneous spray flames are considerably affected by the presence of fuel droplets. In the pre-flame zone, they are enhanced (suppressed) with small (large) latent heat of the liquid fuel.

Besides, there exist heat and mass diffusion in the post-flame evaporation zone when post-flame burning is not considered.

4. The spray flame propagation speed decreases with the Lewis number. For heterogeneous flames, the flame speeds at large flame radius is considerably affected by the Lewis number due to the continuous heat and mass diffusion in the post-flame zone. When the Lewis number is less than unity, the monotonicity of flame propagation speed variation is influenced by droplet loading and/or evaporation rate. Besides, the mass flux magnitude increases with the Lewis number in both pre- and post-flame zones.
5. The Markstein length is affected by droplet loading and evaporation heat exchange coefficient when the Lewis number deviates from unity. Their magnitudes are reduced compared to gaseous flames, which indicates that the degrees of the enhancement or reduction of flame propagation by stretch rate are weakened. Conversely, sensitivity of the Markstein length to the heat exchange coefficient is less pronounced.
6. For heterogeneous flames with post-flame droplet burning, the heat release due to droplet burning leads to higher burned gas temperature and flame propagation speed. The Markstein length is more pronouncedly affected by droplet burning when the liquid fuel loading is relatively low.

SUPPLEMENTARY MATERIAL

See the [supplementary material](#) for the critical and limiting solutions of the theories in the manuscript.

ACKNOWLEDGMENTS

Q.L. is supported by the NUS Research Scholarship.

DATA AVAILABILITY

The data that support the findings of this study are available from the corresponding author upon reasonable request.

REFERENCES

- ¹Y. Mizutani and A. Nakajima, "Combustion of fuel vapor-drop-air systems: Part I—Open burner flames," *Combust. Flame* **20**, 343 (1973).
- ²Y. Mizutani and A. Nakajima, "Combustion of fuel vapor-drop-air systems: Part II—Spherical flames in a vessel," *Combust. Flame* **20**, 351 (1973).
- ³G. D. Myers and A. H. Lefebvre, "Flame propagation in heterogeneous mixtures of fuel drops and air," *Combust. Flame* **66**, 193 (1986).
- ⁴S. Hayashi and S. Kumagai, "Flame propagation in fuel droplet-vapor-air mixtures," *Symp. (Int.) Combust.* **15**, 445 (1975).
- ⁵H. Nomura, K. Izawa, Y. Ujiie, J. Sato, Y. Marutani, M. Kono, and H. Kawasaki, "An experimental study on flame propagation in lean fuel droplet-vapor-air mixtures by using microgravity conditions," *Symp. (Int.) Combust.* **27**, 2667 (1998).
- ⁶H. Nomura, M. Koyama, H. Miyamoto, Y. Ujiie, J. Sato, M. Kono, and S. Yoda, "Microgravity experiments of flame propagation in ethanol droplet-vapor-air mixture," *Proc. Combust. Inst.* **28**, 999 (2000).
- ⁷H. Nomura, I. Kawasumi, Y. Ujiie, and J. Sato, "Effects of pressure on flame propagation in a premixture containing fine fuel droplets," *Proc. Combust. Inst.* **31**, 2133 (2007).

- ⁸F. Atzler, M. Lawes, S. A. Sulaiman, and R. Woolley, in 10th International Conference on Liquid Atomization and Spray Systems ICLASS 2006, 2006.
- ⁹D. Bradley, M. Lawes, S. Liao, and A. Saat, "Laminar mass burning and entrainment velocities and flame instabilities of i-octane, ethanol and hydrous ethanol/air aerosols," *Combust. Flame* **161**, 1620 (2014).
- ¹⁰A. Neophytou and E. Mastorakos, "Simulations of laminar flame propagation in droplet mists," *Combust. Flame* **156**, 1627 (2009).
- ¹¹Z. Ren, B. Wang, D. Zhao, and L. Zheng, "Flame propagation involved in vortices of supersonic mixing layers laden with droplets: Effects of ambient pressure and spray equivalence ratio," *Phys. Fluids* **30**, 106107 (2018).
- ¹²Z. Ren, B. Wang, and L. Zheng, "Numerical analysis on interactions of vortex, shock wave, and exothermal reaction in a supersonic planar shear layer laden with droplets," *Phys. Fluids* **30**, 36101 (2018).
- ¹³P. Jenny, D. Roekaerts, and N. Beishuizen, "Modeling of turbulent dilute spray combustion," *Prog. Energy Combust. Sci.* **38**, 846 (2012).
- ¹⁴G. M. Faeth, "Evaporation and combustion of sprays," *Prog. Energy Combust. Sci.* **9**, 1 (1983).
- ¹⁵P. M. de Oliveira and E. Mastorakos, "Mechanisms of flame propagation in jet fuel sprays as revealed by OH/fuel planar laser-induced fluorescence and OH* chemiluminescence," *Combust. Flame* **206**, 308 (2019).
- ¹⁶S. A. Sulaiman, *Burning Rates and Instabilities in the Combustion of Droplet and Vapour Mixtures* (The University of Leeds, 2006).
- ¹⁷S. A. Sulaiman, M. Lawes, F. Atzler, and R. Woolley, "Effects of droplets on the flame speed of laminar Iso-octane and air aerosols," *Mission. Res. PETROCHEMICAL Catal. Technol.* **5**, 21 (2007).
- ¹⁸R. Thimothee, C. Chauveau, F. Halter, C. Nicoli, P. Haldenwang, and B. Denet, "Microgravity experiments and numerical studies on ethanol/air spray flames," *C. R. Mec.* **345**, 99 (2017).
- ¹⁹R. Thimothee, C. Chauveau, F. Halter, and I. Gokalp, "Experimental investigation of the passage of fuel droplets through a spherical two-phase flame," *Proc. Combust. Inst.* **36**, 2549 (2017).
- ²⁰A. Neophytou, E. Mastorakos, and R. S. Cant, "The internal structure of igniting turbulent sprays as revealed by complex chemistry DNS," *Combust. Flame* **159**, 641 (2012).
- ²¹A. P. Wandel, N. Chakraborty, and E. Mastorakos, "Direct numerical simulations of turbulent flame expansion in fine sprays," *Proc. Combust. Inst.* **32**, 2283 (2009).
- ²²G. Ozel Erol, J. Hasslberger, M. Klein, and N. Chakraborty, "A direct numerical simulation analysis of spherically expanding turbulent flames in fuel droplet-mists for an overall equivalence ratio of unity," *Phys. Fluids* **30**, 086104 (2018).
- ²³T. H. Lin, C. K. Law, and S. H. Chung, "Theory of laminar flame propagation in off-stoichiometric dilute sprays," *Int. J. Heat Mass Transfer* **31**, 1023 (1988).
- ²⁴C.-C. Liu and T.-H. Lin, "The interaction between external and internal heat losses on the flame extinction of dilute sprays," *Combust. Flame* **85**, 468 (1991).
- ²⁵J. B. Greenberg, A. C. McIntosh, and J. Brindley, "Linear stability analysis of laminar premixed spray flames," *Proc. R. Soc. London, Ser. A* **457**, 1 (2001).
- ²⁶J. B. Greenberg, "Finite-rate evaporation and droplet drag effects in spherical flame front propagation through a liquid fuel mist," *Combust. Flame* **148**, 187 (2007).
- ²⁷W. Han and Z. Chen, "Effects of finite-rate droplet evaporation on the ignition and propagation of premixed spherical spray flame," *Combust. Flame* **162**, 2128 (2015).
- ²⁸Q. Li, H. Zhang, and C. Shu, "Propagation of heterogeneous and homogeneous planar flames in fuel droplet mists," *Int. J. Multiphase Flow* **133**, 103452 (2020).
- ²⁹Y. Zhuang and H. Zhang, "On flame bifurcation and multiplicity in consistently propagating spherical flame and droplet evaporation fronts," *Int. J. Multiphase Flow* **125**, 103220 (2020).
- ³⁰N. S. Belyakov, V. I. Babushok, and S. S. Minaev, "Influence of water mist on propagation and suppression of laminar premixed flame," *Combust. Theory Model.* **22**, 394 (2018).
- ³¹W. Han and Z. Chen, "Effects of finite-rate droplet evaporation on the extinction of spherical burner-stabilized diffusion flames," *Int. J. Heat Mass Transfer* **99**, 691 (2016).
- ³²Y. Zhuang and H. Zhang, "Effects of water droplet evaporation on initiation, propagation and extinction of premixed spherical flames," *Int. J. Multiphase Flow* **117**, 114 (2019).
- ³³G. Joulin and P. Clavin, "Linear stability analysis of nonadiabatic flames: Diffusional-thermal model," *Combust. Flame* **35**, 139 (1979).
- ³⁴P. Clavin, "Dynamic behavior of premixed flame fronts in laminar and turbulent flows," *Prog. Energy Combust. Sci.* **11**, 1 (1985).
- ³⁵Z. Chen and Y. Ju, "Theoretical analysis of the evolution from ignition kernel to flame ball and planar flame," *Combust. Theory Model.* **11**, 427 (2007).
- ³⁶Q. Li, C. Liu, H. Zhang, M. Wang, and Z. Chen, "Initiation and propagation of spherical premixed flames with inert solid particles," *Combust. Theory Model.* **24**, 606 (2020).
- ³⁷R. Blouquin, P. Cambray, and G. Joulin, "Radiation-affected dynamics of enclosed spherical flames propagating in particle-laden premixtures," *Combust. Sci. Technol.* **128**, 231 (1997).
- ³⁸R. Blouquin and G. Joulin, "Radiation-affected hydrodynamic instability of particle-laden flames," *Combust. Sci. Technol.* **110-111**, 341 (1995).
- ³⁹Y. Ju and C. K. Law, "Dynamics and extinction of non-adiabatic particle-laden premixed flames," *Proc. Combust. Inst.* **28**, 2913 (2000).
- ⁴⁰W. E. Ranz and J. W. R. Marshall, "Evaporation from drops," *Chem. Eng. Prog.* **48**, 141 (1952).
- ⁴¹L. He, "Critical conditions for spherical flame initiation in mixtures with high Lewis numbers," *Combust. Theory Model.* **4**, 159 (2000).
- ⁴²H. Zhang and Z. Chen, "Spherical flame initiation and propagation with thermally sensitive intermediate kinetics," *Combust. Flame* **158**, 1520 (2011).
- ⁴³H. Zhang, P. Guo, and Z. Chen, "Outwardly propagating spherical flames with thermally sensitive intermediate kinetics and radiative loss," *Combust. Sci. Technol.* **185**, 226 (2013).
- ⁴⁴H. Zhang and Z. Chen, "Effects of heat conduction and radical quenching on premixed stagnation flame stabilised by a wall," *Combust. Theory Model.* **17**, 682 (2013).
- ⁴⁵M. L. Frankel and G. I. Sivashinsky, "On effects due to thermal expansion and Lewis number in spherical flame propagation," *Combust. Sci. Technol.* **31**, 131 (1983).
- ⁴⁶M. L. Frankel and G. I. Sivashinsky, "On quenching of curved flames," *Combust. Sci. Technol.* **40**, 257 (1984).
- ⁴⁷H. Li, H. Zhang, and Z. Chen, "Effects of endothermic chain-branching reaction on spherical flame initiation and propagation," *Combust. Theory Model.* **23**, 496 (2018).
- ⁴⁸A. H. Lefebvre and V. G. McDonell, *Atomization and Sprays* (CRC Press, 2017).
- ⁴⁹Z. Chen, X. Gou, and Y. Ju, "Studies on the outwardly and inwardly propagating spherical flames with radiative loss," *Combust. Sci. Technol.* **182**, 124 (2010).
- ⁵⁰H. Zhang, P. Guo, and Z. Chen, "Critical condition for the ignition of reactant mixture by radical deposition," *Proc. Combust. Inst.* **34**, 3267 (2013).
- ⁵¹J. W. Dold, "Premixed flames modelled with thermally sensitive intermediate branching kinetics," *Combust. Theory Model.* **11**, 909 (2007).
- ⁵²J. B. Greenberg and A. Kalma, "The influence of fuel droplet characteristics on chemical mechanisms in a premixed laminar spray flame," *Int. J. Turbo Jet Engines* **18**, 65 (2001).
- ⁵³S. K. Aggarwal and W. A. Sirignano, "Unsteady spray flame propagation in a closed volume," *Combust. Flame* **62**, 69 (1985).
- ⁵⁴J. B. Greenberg and A. Kalma, "A study of stretch in premixed spray flames," *Combust. Flame* **123**, 421 (2000).
- ⁵⁵C. K. Law, *Combustion Physics* (Cambridge University Press, New York, 2006).
- ⁵⁶M. Lawes, Y. Lee, and N. Marquez, "Comparison of iso-octane burning rates between single-phase and two-phase combustion for small droplets," *Combust. Flame* **144**, 513 (2006).